Conflicts in natural selection constrain adaptation to climate change in *Arabidopsis thaliana*

Megan Ruffley[1*], Laura Leventhal[1,2], Shannon Hateley[1], Seung Y. Rhee[1,2,#], Moises Exposito-Alonso[1,2,3*]

[1]Department of Plant Biology, Carnegie Institution for Science, Stanford, California, USA
[2]Department of Biology, Stanford University, Stanford, California, USA
[3]Department of Global Ecology, Carnegie Institution for Science, Stanford, California, USA
*corresponding authors: meganrruffley@gmail.com, moisesexpositoalonso@gmail.com
[#]New address: Plant Resilience Institute, Michigan State University, East Lansing, Michigan, USA

Keywords: natural selection, multivariate complex traits, genome-wide association studies, evolutionary constraints, *Arabidopsis thaliana,* climate change adaptation

Adaptation to new environments can be impeded if beneficial phenotype combinations cannot coexist due to genetic constraints. To understand how such constraints may hinder plant adaptation to future climates, we compiled a comprehensive database of traits of *Arabidopsis thaliana* and estimated phenotypic natural selection in common gardens in its native distribution with rainfall limitation treatments. We found a natural selection conflict in drought environments as two drought-adaptive strategies, escape and avoidance, are mutually exclusive in *A. thaliana*. Traits underlying such strategies, such as flowering time, growth rate, and water use efficiency, are genetically correlated, and we identify novel loci involved in such correlation experiencing antagonistic natural selection. This empirical evidence shows that these adaptive strategies in natural populations are mutually exclusive due to strong genetic correlations amongst traits that limit the possible combinations of phenotypes. Given projections that future climates will become hotter and drier in many temperate regions, we expect an increasing conflict in natural selection among adaptive traits that could slow down or prevent adaptation. Our study underscores the importance of accounting for evolutionary genetic constraints when predicting how species may respond to a changing climate.

Introduction

Through millions of years of evolution and climatic changes, vascular plants have diversified into almost half a million plant species [1] that vary in an enormous number of life history, physiological, and developmental traits, *i.e.* functional traits [2]. Despite this diversification, a vast majority of phenotype combinations do not exist [3,4]. It is unclear whether those limited combinations of phenotypes are a result of natural selection favoring certain combinations, intrinsic genetic and physiological constraints, or both. Given that climate change will likely surpass 2℃ of global warming and more frequent and extreme droughts are predicted [5–7], and that there is an observed acceleration of functional traits such as early spring phenology [8–10], we must better understand the plausible evolutionary trajectories and constraints hindering future plant adaptation.

Phenotypic trade-offs are common within populations and species as responses to local selective pressures that vary across geographic ranges [11–14]. These trade-offs observed at the phenotypic level may be the result of an underlying genetic correlation amongst traits. Traits can be genetically correlated when there are pleiotropic or tightly linked loci that have large effects in two or more traits at once, and if the correlated allelic effects are antagonistic in phenotypic space, the correlation represents a genetic constraint. The strength of a genetic constraint depends on the polygenicity and heritability of the traits, as these factors, along with selection, determine the rate of phenotypic change, *i.e.* rate of phenotypic adaptation. The quantitative impact of genetic constraints on adaptation at the microevolutionary scale is poorly understood and the information is underutilized when predicting trait evolution [15,16]. Incipient differentiation of phenotypes within populations as a result of local climate differences [11–14] provides an opportunity to understand the environmental drivers and genetic variants constraining ecophysiological and phenological strategies of adaptation [17,18].

Two classically described plant adaptive strategies in response to water limitation are *escape* and *avoidance* [19]. The *escape* strategy refers to changes in temporal life history transitions outside of seasonal drought periods by going through the reproductive cycle quickly, before the onset of drought. In contrast, the *avoidance* strategy aims to maintain internal water pressure by being efficient in CO_2 uptake with simultaneous minimal water loss; often associated with slower growing plants with longer life cycles, and an increase in stomatal density [20]. Different levels of both escape and avoidance strategies have been described in many vascular plant species, especially of annual or short perennial forms, such as *Brassica rapa* [21], wild and domesticated *Lupinus luteus* [22], *Mimulus guttatus* [23], *Arabidopsis lyrata* [24], and *A. thaliana* [25]. In the annual *A. thaliana,* the strategies are functionally mutually-exclusive due to a physiological trade-off between investing resources either in growth to reproduce early (*escapers*) or in water use efficiency strategies (*avoiders*)[13,20,26,27,28]. This trade-off is connected with the slow *vs* fast growth life-history continuum described across plant species and beyond [29].

Water use efficiency (WUE) is generally defined as the efficiency in which CO_2 is fixed relative to water loss and is instantaneously calculated as the ratio of net CO_2 assimilation (A_n) to transpiration (E) rates, two processes highly regulated by stomatal conductance [30]. Measuring instantaneous WUE is difficult in a single experiment because of the time required to measure gas exchange rates accurately for hundreds of individuals. However, overall or lifetime WUE can be characterized using a proxy measure δC^{13}, the ratio of carbon isotope C^{13} to C^{12} found in the leaf relative to atmospheric levels, as it is more fit

for high throughput phenotyping. When stomata are closed, $C^{13}O_2$ is more likely to be assimilated by RuBisCo than when stomata are open, and thus the more often stomata are closed the leaf's isotopic composition will have an overall higher ratio of C^{13}/C^{12} leading to higher δC^{13} and water use efficiency. This ratio captures the leaf's history of closing stomata to avoid water loss and represents a mechanism of dehydration avoidance. Empirical studies have confirmed that δC^{13} is correlated with (A/E)[30–32], assuming similar mesophyll conductance [33] and boundary layer conductance [34] (hereafter WUE refers to measurements of δC^{13}). Unsurprisingly, high WUE of *A. thaliana* accessions is correlated with low annual precipitation in their locations of origin [20]. Despite this putative evidence of local adaptation to low precipitation through dehydration avoidance, higher WUE has not been shown to be associated in *A. thaliana* with increased fitness in common garden experiments simulating water limitation [35], where instead natural selection favors ecotypes that flower early, which is a drought escape strategy and is associated with low WUE[35]. It is true that flowering early has been shown to be adaptive in arid and/or low rainfall environments in *A. thaliana* [36–39], along with several other annual species [22,40,41]. This contradictory evidence implies that selective pressures that drive avoidance and escape phenotypes may be more complicated than previously thought, especially in light of seasonal and yearly fluctuating natural selection on flowering time in Southern range regions [42]. Understanding these nuances in climate influence on adaptive traits will be essential to mapping and predicting rapid adaptation to climate change.

To illuminate the urgent question of whether and how plants may adapt to hot and dry climates, we combined fitness data from common garden field experiments of 515 *A. thaliana* inbred lines developed from natural populations and transplanted in different climates [43], with a curated database of published traits measured in such *A. thaliana* lines [44] and their whole genome sequences part of the 1001 Genomes Project. With this in hand, we (1) characterized the distribution of trait combinations across the *A. thaliana* natural range, (2) examined direct and correlated natural selection pressures on arrays of traits in common gardens, (3) measured heritability and genetic correlations amongst these traits to predict their response to selection, and (4) identified genomic regions containing variants associated with multiple adaptive strategies. This work ultimately reveals a genetic conflict of natural selection between escape and avoidance that could limit population responses to warmer and drier climates.

Results and discussion

A trade-off in *escape* and *avoidance* strategies mirrors Eurasian climatic regions

To understand the phenotypic space of ecological strategies in *A. thaliana,* we gathered trait data related to life history traits and drought response strategies, decomposed the correlated variation to define the primary independent axis of variation, and mapped those axes across the native geographic range. We compiled 1,862 traits measured in greenhouses or growth chambers from 108 published studies that used some subset of accessions from the 1001 Arabidopsis Genomes Project (**Table S1**, **Fig. S1, S2**) [45]. We manually classified traits as either related to escape (125 traits) or avoidance (384 traits) strategies [19,46] (**Fig. S2**), where *escape* traits are related to flowering time, reproduction, growth rate, and dormancy, and *avoidance* traits are related to water use efficiency, stomata, and root architecture. As the accessions measured were partially overlapping across the published studies, we imputed phenotypes in the 1001

Genomes panel taking a machine learning approach with Random Forest (mean normalized RMSE=0.195, **Table S2, Fig. S3**, see **Methods**). To decompose the variation across the trait database, we filtered highly correlated traits and those with less accession coverage, retaining a final set of 64 (**Fig. S4**) for a Principal Component Analysis (PCA). The two main PC axes that explain 23.4% of the total variation (**Fig. 1A, Fig. S5**). The first PC captures a trade-off between WUE and flowering time (highly correlated themselves, Pearson's r = 0.38, p-value < $5x10^{-10}$) (**Fig. 1B**), a trade-off between stomatal density and stomatal size [47], a seed dormancy induction trade-off of fall versus spring germination [48], and a life history shift between rapid flowering and vernalization-required flowering [49]. The second PC is associated with germination rate (*i.e.* primary dormancy) and root architecture, including horizontality (green, **Fig. 1A**) and depth (red-purple, **Fig. 1A**); of secondary focus in this study. The first PC axis is of profound significance and generality, as it is analogous to the first principal component describing the life history, life span, and physiological variation across hundreds of thousands of vascular plant species [4], often called a "fast versus slow" plant economic spectrum [15,50].

The fast-slow PC1 axis summarizes a suite of correlated complex traits involved in seasonal and drought adaptation; a continuum from extreme *escape* to *avoidance* in *A. thaliana* (**Fig. 1A**). This gradient is apparent in trait correlations, as we found that up to 40% of all traits involved in escape or avoidance (n=509) are significantly correlated with flowering time (*i.e.* plant lifespan) [44], 17% correlated with WUE [20], and 25% correlated with growth rate [51] (**Table S3**). PC1 is highly correlated with latitude across the natural range (Pearson's r = 0.35 , p-value < $2.2x10^{-16}$), as are the phenotypes associated with PC1 (**Table S4**) [20,52]. *A. thaliana*'s native populations span from Africa to Scandinavia, thus their populations experience an exceptionally broad climate gradient that has impacts from season lengths to water availability in the soil. To directly visualize and interpret the complex multivariate phenotype-climate relationships across the native range of *A. thaliana*, we conducted a climate-based interpolation of phenotypic variation in PC space using random forest models and maps of 55 climate variables (WorldClim v.2; ref. [53]) for 515 accession localities to predict PC1 (cross-validation accuracy of sample predictions, Pearson's r = 0.73, p-value < $2.2x10^{-16}$) and PC2 (Pearson's r = 0.64, p-value < $2.2x10^{-16}$) variation across the climate of Eurasia (**Fig. 1E**). At first sight, PC1 increases with latitude, with early flowering and late flowering phenotypes representing the extreme latitudes. On the low latitude extreme, populations live in hot and dry climates and flower early (**Fig. 1C**), as it is consistent with accessions from the Mediterranean [42] and North Africa [54]. With short, mild, and wet winters, populations have evolved to not require vernalization [55,56], flower early [54,57]), and rapidly complete their life cycle, canonical of the *escape* strategy to take advantage of a short rainy season. In drought experiments in greenhouses, these early flowering plants have an increased fitness [38,58,59]. At the other, high latitudinal extreme of Scandinavia, populations live in climates with many months of snow cover, germinate in the fall, overwinter as small rosettes, and then have relatively low precipitation during key months of the life cycle from January to May (Pearson's r = -0.15 p-value = 0.047; **Fig. 1D**). The slow, conservative growth leading to late flowering, and the dormant overwintering forced by vernalization requirement genes *FRIGIDA* (*FRI*) and *FLOWERING LOCUS C* (*FLC*), allows for high WUE, a canonical *avoidance* strategy. This makes Northern populations more fit in the field conditions in Sweden [60], and survive longer in greenhouse terminal drought experiments [43].

Many regions of the distribution in Mediterranean and Central European regions are expected to become warmer and dryer [7]. The question is what trait combination are they going to evolve: *escaping*

(early flowering and being wasteful at water use), or *avoiding* (water loss and flowering late). The expectations are unclear, given that high annual temperature is associated with early flowering (Pearson's $r_{flowering\text{-}max.temp.}$ = -0.15, p-value < $5x10^{-4}$; **Fig. 1C**), but low precipitation during the growing season is associated with late flowering (Pearson's $r_{flowering\text{-}mean.precip}$ = -0.14, p-value = 0.002; **Fig. S6**) and high WUE (Pearson's $r_{WUE\text{-}mean.precip}$ = -0.15, p-value = 0.047; **Fig. 1D**) .

Transplanting experiments where flowering time and fitness is measured across accessions often report natural selection favoring early flowering, low WUE genotypes across gardens of *A. thaliana* in different climates [37,42,54,61] (**Table S9**). However, other gardens in warm and dry climates such as Andalucia (South Spain) [62], Valencia (East Spain) [37], or Italy [61], either have identified a positive correlation or no relationship between late flowering and high fitness. Even experiments in the same location showed variable early- and late-flowering-favorable years apparently driven by precipitation regimes [42], suggesting a complex relationship of climate with *escape* and *avoidance* strategies. The difficulty to disentangle these strategies comes from lack of hard phenotypes measured in field conditions, and the lack of climate manipulation approaches in field experiments to attribute natural selection to certain environmental variables.

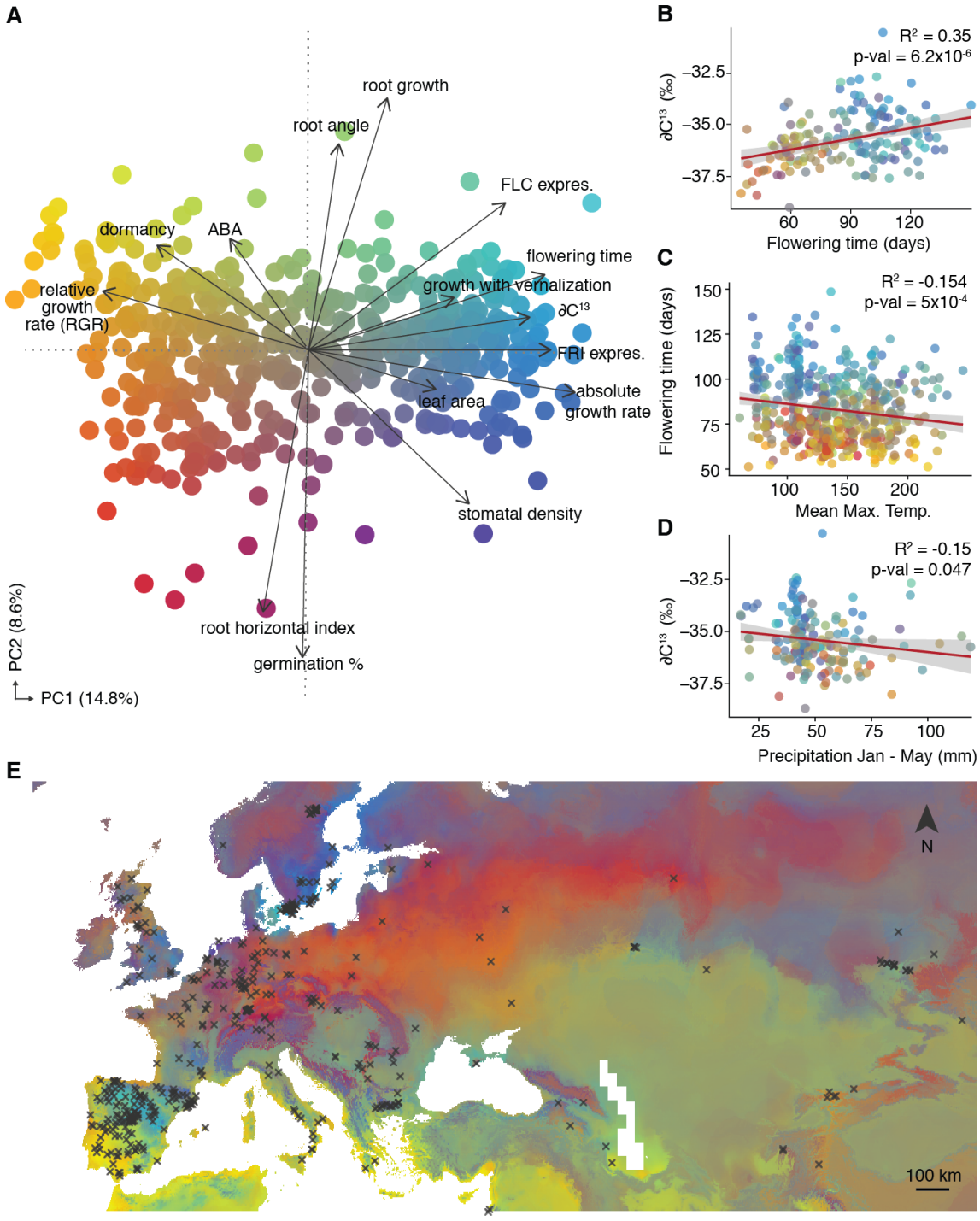

Fig. 1 | Escape and avoidance strategy combinations across the *A. thaliana* populations.

(**A**) Principal Component Analysis (PCA) of 64 key ecophysiological and life history traits (loadings of several key traits are shown in arrows). (**B**) Correlations between flowering time (FT @ 16C) and δC^{13}, (**C**) flowering time and mean maximum yearly temperature (**D**) δC^{13} and precipitation from January through May (**E**) Projection of the expected strategy in PCA of (A) based on a Random Forest niche model of the two-dimensional PC space by local climate in 515 *A. thaliana* accessions (locations of origins shown as crosses).

Natural selection conflict between *escape* and *avoidance* in outdoor experiments with rainfall reduction manipulations.

To disentangle how future challenging climates may select for escape and avoidance strategies, we combine our trait database with fitness measured in outdoor common garden experiments in Spain and Germany with rainfall manipulations [62–64]. In these experiments, 515 geographically diverse *A. thaliana* accessions [44] were scored for viability (survival to reproduction) and fecundity (number of offspring of surviving plants) in the two locations, with a high and low watering treatment within location, and a high and low plant density within watering treatment [64]. This resulted in 8 environmental combinations and 24 fitness measurements (including three fitness components of viability, offspring, and the combination). We used these fitness data to estimate total selection coefficients s (*sensu* Lande & Arnold, ref. [65]) for phenotypes as the covariation between relative fitness w and the given phenotype z, $w = sz$. Specifically, we independently quantified phenotypic selection coefficients for 1,823 traits and 20 PC axes explaining 75% of the phenotypic variation [62–64] (analyses were repeated using survival, fecundity, and compound lifetime fitness for all experimental locations and treatments (**Table S6**)). This revealed that the first phenotypic axis (PC1, i.e. early-to-late flowering strategy) had the most significant, negative associations with fitness (17 out of 24) (**Table S7**), reinforcing that the early flowering escape strategy is favored by natural selection in both Mediterranean and Central European sites.

Such correlation of PC1 and fitness was also patent in the most stressful hot-dry-high-plant-density environmental condition in Spain ($s_{fitness}$ = -0.152, p-value$_{boot}$ < 1.0x10^{-3}), and was also clear in individual correlations of the major traits underlying PC1: early flowering ($s_{fitness}$ = -0.110, p-value$_{boot}$ < 1.0x10^{-3}; **Table S8-9**), fast growth ($s_{fitness}$ = -0.176, p-value$_{boot}$ < 1.0x10^{-3}; **Table S10**), high seed dormancy ($s_{fitness}$ = 0.129, p-value$_{boot}$ < 5.0x10^{-2}; **Table S11**), and low WUE ($s_{fitness}$ = -0.110, ns; **Table S12**). This corroborates some of the aforementioned published results from outdoor field experiments [37,42,61], but in-depth analysis of PC1's association also revealed the striking switch in correlation from negative when utilizing only survival as fitness ($s_{survival}$ = -0.372, p-value$_{boot}$ < 1x10^{-3}), to positive utilizing only fecundity as fitness ($s_{fecundity}$ = 0.109, p-value$_{boot}$ < 5x10^{-2}, **Table S7**); insinuating the potential conflict known in ecology where later phenology increases the ability of plants to accumulate resources for reproduction but risk an increased mortality [66]. We also observe this pattern with flowering time associated with survival (**Fig 2A**), fecundity (**Fig 2B**), and lifetime fitness (**Fig. 2C**) data (ref. [64]), where the hot and dry environment shows survival favoring early flowering (**Fig. 2A**), but high fecundity associated with late flowering (**Fig. 2B**), and lifetime fitness appears to be a combination of the prior two measures (**Fig. 2C**).

Because the plant lifespan principal component (PC1) is influenced by multiple correlated adaptive traits involving escape and avoidance, we aimed to better disentangle natural selection measurements by quantifying *direct* effects of natural selection in each trait accounting for trait correlations using multivariate selection analyses [65]. We then estimated: $\beta = P^{-1}s$; s is the previously quantified total selection coefficient (without accounting for correlations), where P is the variance-covariance matrix among phenotypes, and β is the "gradient of selection" (or direct selection), which captures natural selection over a trait that cannot be attributed to their correlations with other traits.

For computational efficiency, we narrowed down from 64 to 12 key focal traits measured in growth chambers (with a minimum coverage of 43 accessions, and mean of 180) (**Table S13**): ABA accumulation in leaf (ref. [67]), WUE measured as δC13 (ref. [20]), primary dormancy (DSDS50; ref. [68]), secondary dormancy based on germination after 8 days in ℃ (d8_10C_perc; ref. [48]), flowering time at 16 ℃ (ref. [44]), absolute growth rate and relative growth rate (RGR) (ref. [51]), flowering after long day and vernalization (ref. [49]), root horizontal index and root RGR (ref. [69]), and stomatal density and size in fully developed leaves (ref. [20]) (see trait correlation matrix **Fig. S7**).

When studying the consistency between total and direct selection over traits in the hot and dry environment (**Figs. 2D, S8**), we identified a primary congruent negative direct selection pressure over growth rate ($s_{fitness}$ = -0.185, p-value$_{boot}$ < 1.0x10^{-3}; $\beta_{fitness}$ = -0.209, p-value$_{boot}$ < 1x10^{-3}; **Table S14**), where selection favors low absolute growth rates, suggesting selection for the *escaping* strategy. However, in addition we found an incongruent direct selection over late flowering time (*avoiders)* once we accounted for trait correlations ($\beta_{fitness}$ = 0.184, p-value$_{boot}$ < 1x10^{-3}; **Table S14**), even in survival ($\beta_{survival}$ = 0.19, p-value$_{boot}$ < 1x10^{-3}) (**Fig. 2A, D**). While a positive $\beta_{fitness}$ for flowering time may be due to the influence of fecundity on lifetime fitness, the positive $\beta_{survival}$ reveals there is also a survival advantage in addition to larger seed sets. These analyses are evidence that the apparent correlation of fitness with early flowering is a spurious one that not only vanishes but reverses when accounting for trait correlations (we attributed this to growth rate and vernalization using a leave-one-out approach, **Fig. S9**).

WUE, which counterintuitively strongly correlated with low survival in a hot-dry environment at both low plant density ($\beta_{survival}$ = -0.112, p-value$_{boot}$ < 1x10^{-3}) and high plant density ($\beta_{survival}$ = -0.192, p-value$_{boot}$ < 1x10^{-3}, **Table S14**), became non-significant while accounting for trait correlations (**Fig. 2D**). Moreover, WUE in Germany, which was non-significantly related with survival in well-watered conditions (**Fig. 2E, Table S15**), became positive in the experimental treatment in Germany where a Spanish low precipitation was imposed ($s_{survival}$ = 0.027, p-value$_{boot}$ < 5x10^{-2}; even after correcting for flowering time effects, $\beta_{survival}$ = 0.075, p-value$_{boot}$ < 1x10^{-3}; **Fig. S10**). These analyses provide evidence of a conflict in natural selection between two adaptive strategies to water limitation in realistic outdoor climates that may lead to inefficient phenotypic evolutionary responses [18,66].

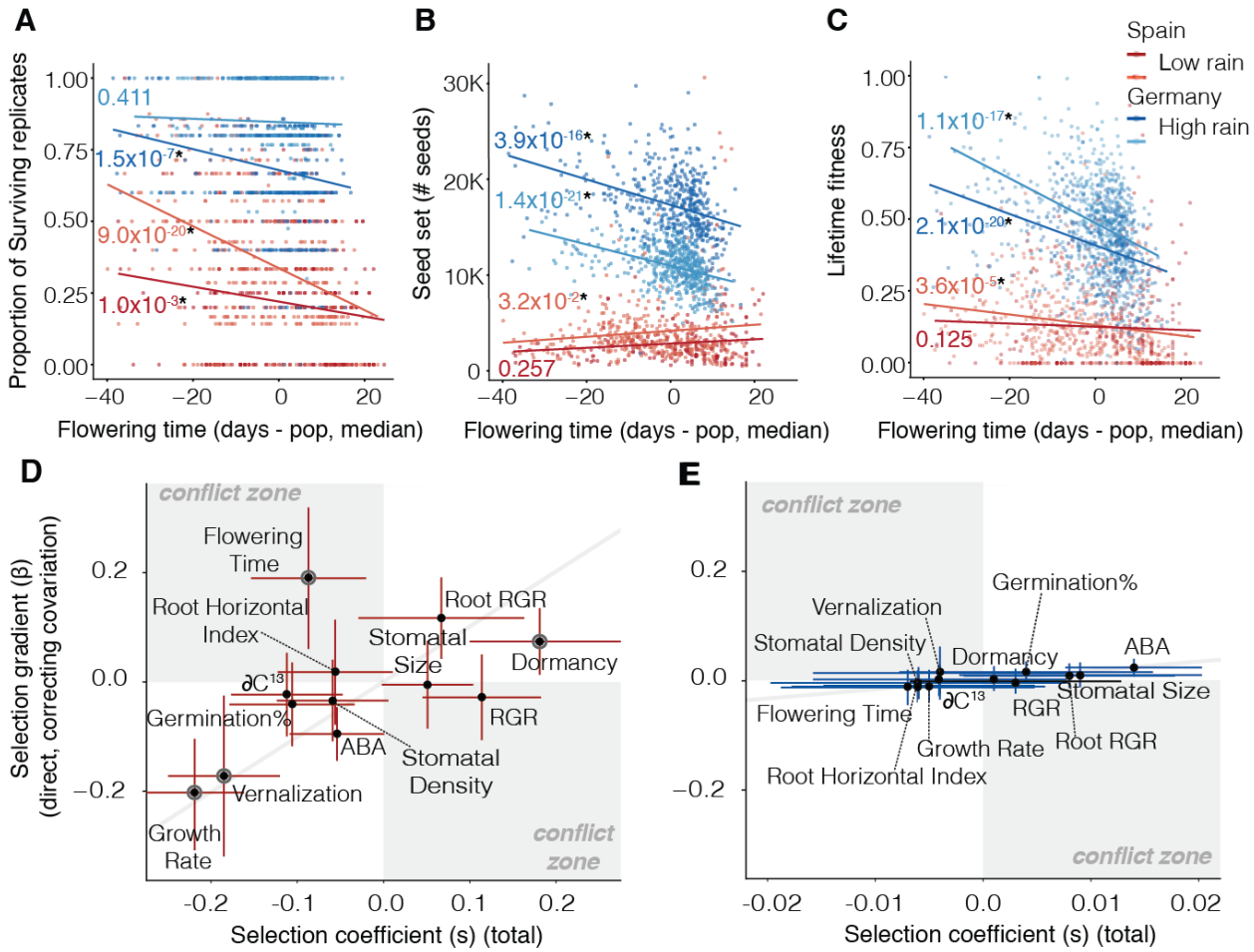

Fig. 2 | Conflicts in natural selection over escape and avoidance traits.

Phenotypic selection is measured as the absolute correlation between flowering time (median-centered flowering time in this case) and **(A)** survival proportion, **(B)** number of seeds set, and **(C)** relative lifetime fitness (normalized 0-1 for visualization). Associated P-values are in the same color as trend lines (**D**) Total selection coefficients (*s*) vs. direct selection gradients (β, after accounting for trait covariation), using survival data from the hot and dry common garden experiment (Spanish field site). Large circles indicate significance of β and s ($P < 0.05$) and gray areas indicate a conflict where total selection is in one direction (+/-) while direct selection is in the opposite direction. (**E**) Same as (D) but using fitness in the cold and wet common garden (Tubingen field site).

The joint genetic basis of escape and avoidance strategies constrain phenotypic responses.

Because we documented natural selection in outdoor field experiments with water limitation over two different strategies that showed antagonistic correlations at the phenotype level, *escape* and *avoidance*, we then wondered whether such correlation also manifests at the genetic level potentially constraining evolution of both strategies [17,18,70]. We then performed systematic genome-wide associations (GWAs) with 515 *A. thaliana* accessions for each of the 1,862 phenotypes using a linear mixed model [71]. In addition, we performed multivariate mixed model genome wide association (mGWA) for the pairs of the 12 target

phenotypes used in phenotypic selection analysis [72] (**Fig. 2D, E**). We found that the majority of traits had moderate-to-high SNP-based heritability h^2 = 0.54 [0.17-0.71]) and were highly polygenic (gamma n parameter = 49.47 potentially causal loci [19.2-68.7]) (**Table S16**). Moreover, *escape* traits had higher heritability estimates (mean h^2 = 0.71 [0.43-0.99]) than *avoidance* traits (mean h^2 = 0.49 [0.03-0.94]) (wilcox test p-value=2.6×10^{-8}, **Fig. S11**). Genetic correlations within *escape* traits such as flowering time and growth rate were high and positive ($r_{g\text{-flowering-growth}}$= 0.45, 95% CI 0.38–0.52; **Fig. S12**), but these traits were also strongly correlated with *avoidance* traits such WUE ($r_{g\text{-flowering-WUE}}$= 0.34, 95% CI: 0.26–0.42, **Fig. 3A**; $r_{g\text{-growth-WUE}}$= 0.33, 95% CI 0.25–0.42; **Fig. S13**). We then used the breeder's equation (*sensu* Lande & Arnold, ref. [65]) to predict the average phenotype change of each trait as: as $\Delta z = GP^{-1}s$, where G is the additive genetic variance-covariance matrix constructed from heritability and genetic correlation estimates among 12 traits, P is the phenotypic variance-covariance matrix, and s is the raw covariance of the trait with lifetime fitness in hot-dry conditions. Only traits with consistent phenotypic selection coefficients (s) and direct gradients (b) (**Fig. 2D**), such as growth rate, were predicted to evolve. As we suspected, flowering time and WUE are not expected to evolve in any direction, rather we predict the counterintuitive "evolutionary stasis" of these traits in a Mediterranean climate with water limitation ($\Delta z_{\text{flowering}}$=0.136, p-value > 0.05; Δz_{fWUE}=-0.044, p-value > 0.05, **Fig. 3D, Fig. S14, Table S17**).

To further investigate the phenotypic effects in flowering time and WUE of specific genomic loci and their signatures of natural selection directly at the genetic level, we focused on the top 0.05% SNPs (274) of the multivariate GWA. This showed a strikingly parallel pattern, where alleles increasing WUE also increased flowering time, and vice versa (Fisher's Exact Test odds ratio 2.7×10^{-4}, p-value < 2.2×10^{-16}; **Fig. 3B**), corroborating an independent evolutionary trajectory of these traits is likely not feasible. Likewise, the projected allele frequency changes (**Fig. 3C**) also implies evolutionary stasis as the changes in allele frequency are agnostic to the combined effect of the loci. We also identified alleles previously reported to be pleiotropic for flowering time and WUE with knock-out studies of the gene *FRIGIDA* [35], (**Fig. S15**), and also discovered a highly significant novel locus in chromosome 1 that had not been described before (this locus was consistently a top hit in GWA with imputed [n=1,135] and non-imputed phenotypes [n=248], pruning low frequency or low genotyping SNPs, utilizing kinship correction as well as 5 genomic PC covariates, see **Fig. S16**). The peak of top SNPs in chromosome 1 spans ~7.5Kbp and overlaps with 5 candidate genes (AT1G11500-AT1G11540) (**Fig. S17, 18)**. While many of these genes do not have their molecular function or impact on biological processes fully characterized, they are involved in leaf development and determination of bilateral symmetry (AT1G11500), a transcription regulator (AT1G11510), a protein involved in disulfide isomerase activity (AT1G11530), a sulfite exporter TauE/SafE family protein involved in protein ubiquitination and highly expressed in the root (AT1G11540), and one with completely unknown molecular functions (AT1G11520) (**Tables S18-19**). Notably, in the mGWA from imputed flowering time and WUE data, only AT1G11540 and two additional genes contained highly significant alleles near the Chr 1 peak, one associated with embryo development ending in seed dormancy (AT1G11680), and the other involved in a cellular macromolecule metabolic process (AT1G11740) (**Tables S20-21**). The expression of three of these genes correlate with flowering time and only AT1G11540's expression correlates with WUE (**Fig. S19**) (transcriptome data from the 1001 Genomes consortium, ref. [73]).

While mechanistic links need to be elucidated, we could estimate the effect of natural selection by associating SNPs with fitness traits as in a regular GWA with fitness [64]. We found the alleles on the chromosome 1 peak, which increased both flowering time and WUE (**Fig. 3B**), were negatively correlated with lifetime fitness (mean effect size = -0.054[0.10]; **Fig. 3A**), but after correcting for growth rate as a cofactor in the fitness GWA, their correlation with fitness reversed (mean effect size = 0.173[0.190]; **Fig. 3A**). Such alleles also correlated negatively with survival (mean effect size= -0.117[0.089]) but positively with fecundity (mean effect size= 0.089[0.070]). We speculate a novel causal locus in the region (or multiple effectively indistinguishable loci in a few Kbp proximity) has pleiotropic functional effects in multiple traits, and is subject to antagonistic selection at different life stages leading to a fitness conflict.

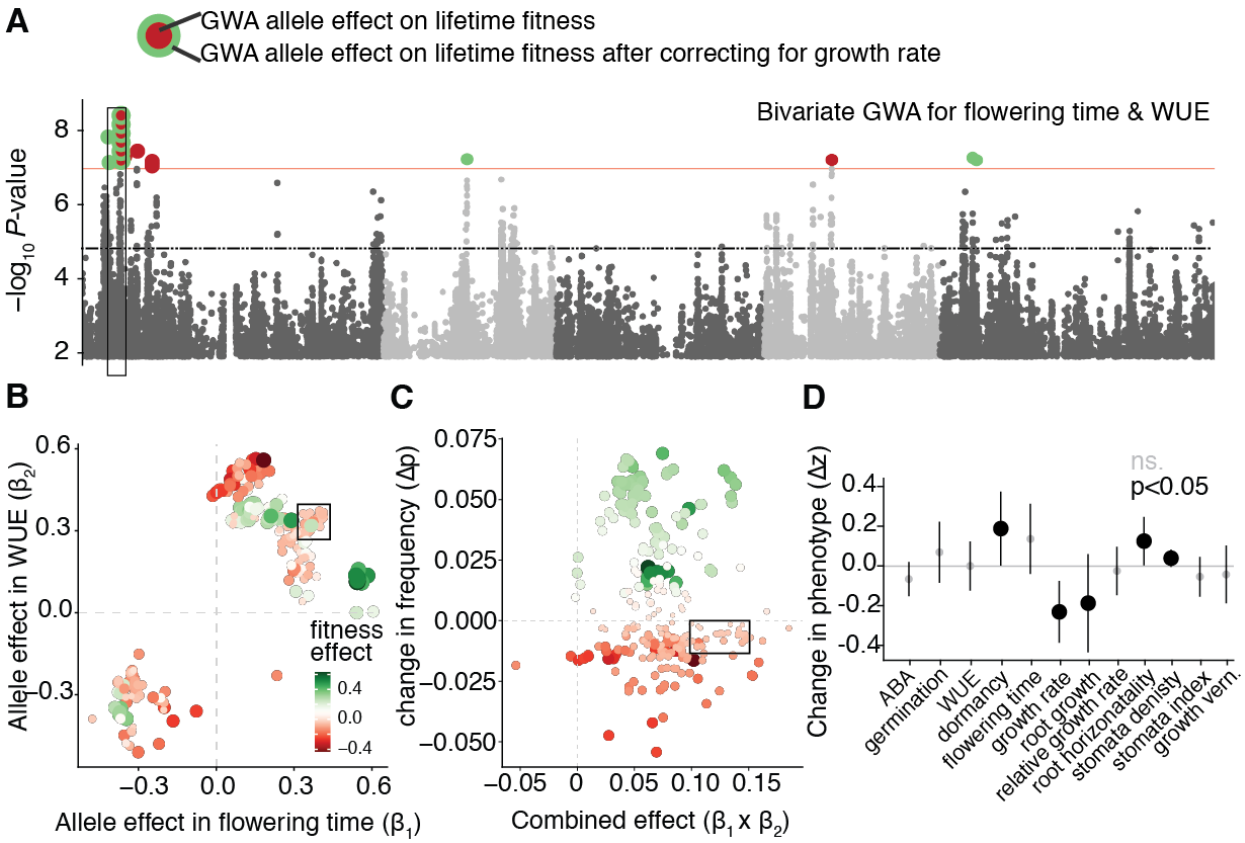

Fig. 3 | Genetic architecture of escape and avoidance traits and the consequences of natural selection in a water limited experiment.

(A) Multivariate Genome-Wide Association (mGWA) of flowering time and WUE with annotated genes passing a genome-wide significance threshold of $-\log_{10}$ *P*-value > 7.03. Significantly associated SNPs are colored based on the effect size of a GWA with lifetime fitness from a hot and dry environment, indicating alleles favored (green) or disfavored (red) by natural selection. The outer color of the same alleles indicates effect size direction of lifetime fitness after correcting for growth rate. Dashed black line indicates inclusion in the top 0.05% of alleles, $-\log_{10}$ *P*-value > 5.13. **(B)** Top 0.05% SNP effect sizes (ß) from mGWA of flowering time and WUE (n=247) from (A, above dashed line), points colored and sized by allele effects on fitness estimated from GWA of lifetime fitness in the hot and dry environment. (**C**) Expected allele frequency change in response to selection in relation to alleles' joint effect on WUE and flowering time. (**D**). Predicted mean phenotypic response to selection across traits.

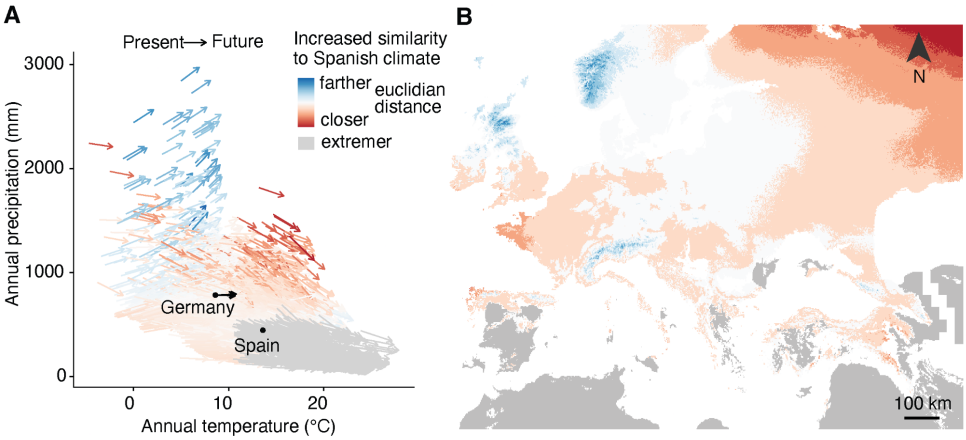

Fig. 4 | Climate change trajectories lead to conflict in phenotypic evolution

(A) Change in annual precipitation and temperature similarity to the Spanish field site climate in 2050 (measured as euclidean distances). (**B**) Map of climate trajectories in (A). Climate maps were retrieved from Max Planck CMIP5 IPCC projections of business-as-usual scenarios (worldclim.org). Gray areas indicate regions whose temperature will increase and while precipitation will decrease below the average precipitation at the Spanish field site location (*i.e.* more extreme conditions).

Conclusion

Global warming is a strong selection force that will push plants to evolve or otherwise perish. However, understanding plausible adaptive phenotypic evolutionary trajectories is challenging from simple correlations between observed phenotypes and climates. Utilizing phenomic and genomic resources of *A. thaliana*, a machine learning data integration, and outdoor field experiments, we showed that rainfall limitation may lead into an evolutionary conflict between accelerating the plant life cycle (*escape*) and optimizing water use efficiency (*avoidance*); leading to an evolutionary stasis of phenotypic change. Climate trajectories in Europe can exacerbate this evolutionary trade off (**Fig. 4**). Given the ongoing observation that many plant species are accelerating flowering time [8–10] and the universality of escape and avoidance strategies across plant clades [74], we should expect evolutionary constraints to impose limits to adaptation. Our work emphasizes the need to understand natural selection conflicts and genetic constraints when predicting species responses to future climates.

Methods

Mapping the phenotypic landscape of *Arabidopsis thaliana*

Data curation

The assembled phenotype database comes from a combination of laboratory and field experiments that use a subset of the 1001 Genomes *A. thaliana* accessions. Nearly 600 phenotypes come from the Arapheno database (Seren et al. 2017), and the remainder were compiled by Voichek & Weigel (REF) and ourselves from published literature (See **Supplemental Tables**). Fitness data comes from outdoor field experiments in 2 locations with rainfall and density treatments [64]. In total, data from 1,862 phenotypes were gathered from over 108 published sources (**Table S1**). In the case of replicated ecotypes within an experiment with multiple measures for the same phenotype, we took the mean of the replicates. We classified every trait into a general functional category (**Fig. S2A**), and classified 1,282 traits as being related to one of three drought adaptation strategies; *escape*, *avoidance*, and *tolerance* (**Fig. S2B**; Kooyers 2015). We classified escape traits as those that contribute to germination, growth, and reproduction. This encapsulates traits related to dormancy induction and germination rate, growth rate, vernalization, and all traits related to reproduction, importantly flowering time. Avoidance traits were classified as those that are related to preventing drought with advantageous phenotypes that both conserve and increase access to water, including root growth and angle related traits, leaf area, biomass accumulation, stomatal density and size, and δC^{13}. Tolerance traits were annotated as those involved with enduring low water content such as increased production of osmolytes and other metabolite related phenotypes, as they may play an important role in desiccation tolerance and osmotic regulation. While tolerance may be an important ecological strategy for Arabidopsis in another context, we do not focus on these traits in this study. We used the R package *missForest* to fully impute the trait dataset [75]. This was done iteratively for each trait and all 1,135 individuals, with all other traits being used as predictors. The out-of-bag approach resulted in an average normalized root mean squared error (NRMSE) of 0.195 (**Fig. S4**) and an estimated NRMSE for all traits (**Table S2**). The imputation was necessary for many of the subsequent analyses performed with the traits, such as the principal components analysis (PCA), estimation of selection coefficients, and multivariate GWAS.

These traits were measured in many different experimental environments, introducing variation that could impact our overall inference if phenotypes are highly variable across experiments. To evaluate if this would be a concern, we correlated values for the same traits that were measured in 15 experiments/studies to verify if accessions are consistent in their relative positions in trait distributions across experiments. Given the high correlations measured (**Fig. S20**) we expect these differences and ranks among accessions to be relatively consistent.

Principal Components Analysis

We used principal components analysis (PCA) to decompose the variation of traits in a subset of 515 accessions for which field fitness data was available. We first isolated specific traits related to seed dormancy, vernalization, germination, flowering time, leaf traits, roots, stomata, growth rates, and stress response. This narrowed down the traits to 205. We then removed highly correlated traits ($R^2 > 0.7$), resulting in a total of 64 (**Fig. S4**). After scaling traits, the 515 accessions and 64 traits were then used in the primary PCA (**Fig. 1A**). To ensure the pattern we observed with a subset of the accessions was consistent with the entire species we also performed a PCA using all native Eurasion accessions from the 1001 genomes project (n=999) (**Fig. S5**).

Trait associations and climate projections

We measured how many of all traits were correlated with flowering time, WUE, and growth rate using the Pearson's correlation coefficient with a significance threshold of 0.05 and the non-imputed dataset (**Table S3**). Using the latitude of the original collection location associated with the focal 515 *A. thaliana* accessions, we also estimated Pearson's correlation coefficient for the target 64 traits and the main two PC axes with latitude (**Table S4**). We downloaded bioclimatic, temperature, precipitation, and evapotranspiration rate estimates from WORLDCLIM 2.0 for all the localities associated with the 1001 genomes accessions. We again subsetted the accessions to the 515 for which we have fitness data available, and estimated Pearson's correlation coefficient between climate data and target traits (**Table S5**). We fit linear regression models of the climate data as a function of these target traits. We did this

first exclusively with the climate data and traits, and then with genomic principal components (PCs) from the 1001 genomes project accessions and latitude as covariates in the model (**Fig. 1C-D**).

Using *randomForest*, we constructed two climate models to predict the phenotypic landscape of PC1 and PC2 across the entire range of *A. thaliana*. To build the models, we used climatic data (temperature, precipitation, and bioclimatic variables; 55 total) associated with the localities of the focal 515 accessions to predict PC1 and PC2. These models used 1000 decision trees. The predicted values of PC1 and PC2 for every map grid in Eurasia from longitude 15W to 90E, and latitude 34N and 65N were visualized after normalization as HUE (**Figure 1A)**. We also estimated the accuracy of the random forest predictions of PC value by performing cross-validation using two thirds of the data for training and one third for testing. We then estimated the accuracy of the models by correlating the predicted values with the true values for the respective PCs.

Measuring direct and indirect selection

Selection coefficient estimation (total= indirect + direct)

We measured phenotype selection on all traits of this study (n=1,823) and 20 PC axes. To compute phenotypic selection coefficients *s* (Lande and Arnold 1983), we use covariation between relative lifetime fitness *w* (number of offspring including 0s divided by the mean of the population) and a given phenotype z (mean and variance centered): $w = sz$, where s is the total selection coefficient. For each trait, we computed s with 100 bootstrap replicates with replacement. Traits with a significant association with selection were determined as those with estimates whose 95%, 99%, and 99.9% CI does not overlap with 0, denoted as *, **, and ***, respectively. In order to compare these measures of selection, all fitness measures and traits were scaled prior to calculating their covariance. The fitness data was measured in two different environments, Madrid, Spain (m) and Tubingen, Germany, (t) in two rainfall treatments at each location high (h) and low (l), as well as two planting densities, population (p) and individual (i). This resulted in a combination of eight different treatments: mhp, mhi, mlp, mli, thp, thi, tlp, tli. For each treatment, three fitness traits were measured: survival, seeds set, and lifetime fitness. All were used to detect an association with selection for all traits (**Table S6-12**).

Selection gradient estimation (direct, after multivariate correction)

To understand the direct effects of natural selection on traits, we accounted for correlations amongst traits using the multivariate selection approach: $\beta = P^{-1}s$, where P is the phenotypic variance-covariance matrix [65], s is the previously quantified total selection coefficient (without accounting for correlations), and β is the gradient of selection (or direct selection) that captures the independent effects of each trait that cannot be attributed to their associations with other traits. Through a series of trait imputation, decorrelation, and expert selection, we narrowed the analyses to 12 focal traits related to both seasonal and drought adaptation (**Fig. S7**). In addition to the fitness data from Exposito-Alonso et al. (ref. [52]), we used fitness data from additional common garden experiments using *A. thaliana* in varying environments: Fournier-Level et al. (ref. [63]) (**Fig. S21**) and Manzano-Piedras et al. (ref. [62]) (**Fig. S22**) (**Table S13**). As before, we performed 100 bootstrap replicates with replacement to establish significance of β (direct selection) estimates.

Multivariate prediction of phenotypic response to selection

We inferred the population responses to this natural selection by using the "Breeder's" or selection response equation (ref. [49]): $\Delta z = GP^{-1}s$, where G is the additive genetic variance-covariance matrix constructed from heritability and genetic correlation estimates among 12 traits, P is the phenotypic variance-covariance matrix, and s is the raw covariance of the trait with lifetime fitness in hot-dry conditions. For this, we used the estimates of s from lifetime fitness in both the hot-dry environment (Madrid (m) and low water (l)) and the cool-wet environment (Tubingen (t), high water (h)), for both individual (i) and population (p) planting densities. For the genetic variance-covariance matrix, we used the SNP-based heritability estimates with target phenotypes using a linear

mixed model GWA (**Table S16**), and the genetic correlations estimated from multivariate GWA (**Fig. S13**). Estimates of phenotypic change are thus reported for the four environments above (**Fig. S14**).

Climate projections

We downloaded the averaged historical (1970-2000) bioclimatic variables [53] for Eurasian range of *A. thaliana* at 5 km^2 (2.5 minutes) resolution. Future predicted climate was retrieved from the Max Planck CMPI5 IPCC model projections of a business-as-usual scenario [53]. We plotted the 1970-2000 average value of annual precipitation and mean annual temperature as the beginning of the arrows (**Fig. 4A**) and the 2050 predicted values as the end of the arrows to indicate the trajectory of the climate in precipitation and temperature space. Arrows indicate whether the euclidean distance (of both temperature and precipitation) between the current and 2050 climates becomes more similar to the current Spanish climate (red) or more dissimilar (blue) (**Fig. 4A**). Trajectories with predicted precipitation and temperature more extreme than the Spanish site are in gray (**Fig. 4B**).

Genetic architecture of traits and genetic correlations

Genome wide associations

Before we performed genome-wide association studies (GWAS), we quantile transformed all trait data that were continuous values as using quantile transformed trait data in GWAS has shown to reduce type 1 error rates compared to non-normal, untransformed values [76]. For count data and traits with many zeros, we first performed a log(x+1) transformation, followed by a quantile transformation. Binary phenotypes were not transformed. We assessed whether the correlation structure of the phenotypes remained consistent with the imputation and quantile normalization (**Fig. S23**).

To perform genome wide associations (GWA), we started with the 1,135 wild strain accessions and 11,769,920 SNPs generated from the 1001 Genomes Project (1001 Genomes Consortium 2016), however depending on the trait data coverage, not all samples and SNPs were used in every GWA. We ran GWA on all traits using the raw data, normalized data, and imputed data. For each trait we conducted GWA using a univariate linear mixed model (LMM) implemented in the software GEMMA (ref. [71]). This model corrects for genome-wide background differentiation colinear to the phenotype of study (i.e. relatedness and population structure correction). No minor allele frequency cutoff was used unless stated. Following the GWA with the various trait datasets, we compared the estimates of effect sizes across the various datasets using Pearson's correlation coefficients to assess how the data imputation and normalization impacted the ranks of effect size estimates (**Fig. S24**).

Additionally, using the original imputed SNP matrix from http://arapheno.1001genomes.org that contains 10,709,466 SNPs, we subsetted to 1,353,386 SNPs for all 1,135 *Arabidopsis thaliana* wild accessions to be used in a Bayesian sparse linear mixed model (BSLMM) GWA, also implemented in the software GEMMA (Zhou and Stephens 2014), for each of the 1,846 phenotypes. The BSLMM full model is a derivation of LMM, but unlike the LMM that assumes the effect sizes of SNPs are normally distributed, the BSLMM implements two random effect distributions: effect sizes are either attributed to direct effects, that is those that directly affect the trait and are normally distributed with broad variance, and indirect effects, that is background effects that all SNPs have with a narrow variance.

Measures of SNP-based heritability for each trait were estimated using the random effect of LMM informed by the kinship matrix. This essentially quantifies how much genome-wide relatedness explains the variation in the phenotype. We estimated heritability of the traits (raw, normalized, and imputed) and multiple algorithms (LMM and BSLMM) and compared their consistency (**Fig. S25-26**).

Genetic Correlations

Summary statistics

We approximated genetic correlations among traits using Pearson's correlation of summary statistics of SNPs from univariate GWA. We summarized effect sizes of SNPs as Z scores where $Z = (\frac{\beta}{se})^2$. For this approximate genetic correlation, we only correlated unlinked SNP effects by randomly selecting SNPs from independent linkage blocks that had high confidence variant calling, resulting in ca. 60K SNPs. With these approximate genetic correlations, we assessed how consistent genetic correlations were with phenotypic correlations for all traits, only escape traits, and only avoidance traits (**Fig. S27**). We also used genetic correlations estimates from multivariate GWAs of various trait combinations to validate such approximated genetic correlations and the effect of imputed and non-imputed phenotypes (**Fig. S13**).

Multivariate GWA

Multivariate linear mixed effect models were run pairs of the 12 target traits used in phenotypic selection analyses, for which there were enough overlapping trait data (16/66 total traits pairs; **Fig. S13**). These were linear multivariate mixed models run in GEMMA [72], with an allele frequency cutoff of 0.05, 5% missing genotype data maximum, and correlated effects of SNPs corrected for using a kinship matrix. In the case of flowering time and WUE, there were 248 overlapping samples with trait data for both traits, and after passing thresholds, 546,668 biallelic SNPs remained and were associated with the two traits (**Fig. 3A**). We also estimated effect sizes using five genetic PCs as covariates to control for background structure in the model, which marginally improved QQ plots (**Fig. S28**). For flowering time and growth rate, there were 395 samples overlapping and 347,257 SNPs were used (**Fig. S12**). In addition to the mGWA runs of 16 pairs of traits with enough accession overlap, we also conducted mGWAs for all 66 traits pairs using the imputed phenotypes (**Fig. S13**). This was necessary to conduct multivariate phenotypic responses.

For visualization purposes, the SNPs with top 0.05% effects on both flowering time and WUE (from mGWAs) were plotted against the expected allele frequency change (Δp) based on their correlation with lifetime fitness (**Fig. 3C**). We then used as $\Delta p = p(1 - p)a$, where p is the starting allele frequency, and a is the estimated allele effect in fitness based on the relative fitness of the major and minor genotypes in our outdoor experiments (ref. REF, see below).

Allele effects on fitness

A univariate LMM GWA was conducted with fitness measured in outdoor experiments [64] using data for 515 *A. thaliana* accessions. We use the sign of the effect size estimates for each allele to color alleles green and red for positive and negative selection, respectively (**Fig. 3A, B, C**). To exclude that fitness variation explained by growth rate would be attributed to alleles, we conducted a LMM GWAs based on the residuals of a previous linear regression model fitting fitness with growth rate (**Fig. 3A**).

Additional information

Data availability. The 1,864 phenotypes imputed for 1,135 wild *Arabidopsis thaliana* strains are available at github.com/ruffleymr/Athaliana_Natural_Selection_Conflict/data. The data from the 1001 Genomes of *Arabidopsis thaliana* are available at 1001genomes.org. The seed collection can be obtained at the Arabidopsis Biological Resource Center (ABRC) under the ID CS78942. The code to reproduce analyses and figures is available at github.com/ruffleymr/Athaliana_Natural_Selection_Conflict.

Acknowledgements. We are thankful to Moi Lab members, Rhee Lab members, and Oliver Bossdorf for comments and discussion. This work is supported by the Office of the Director of the National Institutes

of Health's Early Investigator Award with award # 1DP5OD029506-01 (M.E.-A.); by the U.S. Department of Energy, Office of Biological and Environmental Research, grant # DE-SC0021286 (M.E.-A., S.Y.R.), DE-SC0018277 (S.Y.R.), DE-SC0008769 (S.Y.R., M.R.), DE-SC0023160 (S.Y.R.); by a USDA NIFA, grant # 2022-67019-36366; and by the U.S. National Science Foundation's DBI grant # 2213983 (Water and Life Interface Institute (WALII)) (S.Y.R., M.E.-A.); and by the Carnegie Institution for Science (M.E.-A., S.Y.R.). M.R. is supported by the National Science Foundation Plant Genome Project as a postdoctoral fellow (Grant No. 2109868). L.L. is supported by the National Science Foundation Graduate Research Fellowship (Fellow ID: 2020304890). S.H. is supported by Stanford's Center for Computational, Evolutionary, and Human Genomics. The analyses that were conducted here used the High-Performance Computing clusters Calc and MoiNode supported by the Carnegie Institution for Science. This work was done in part on the ancestral land of the Muwekma Ohlone Tribe, which was and continues to be of great importance to the Ohlone people.

Author contribution. M.E.-A. and M.R. conceived the project. M.R., L.L., S.H., and M.E.-A. conducted analyses and interpreted results. M.R., L.L. S.H., S.Y.R., M.E.-A interpreted analyses and discussed results. M.R. and M.E.-A. wrote the manuscript with the input of all authors.

Disclosure statement. The authors declare no competing financial interests. The funders had no role in study design, data collection and analysis, decision to publish, or preparation of the manuscript.

References

1. Royal Botanic Gardens, Kew. The State of the World's Plants. (2016).
2. Diaz, S. *et al.* The plant traits that drive ecosystems: Evidence from three continents. *J. Veg. Sci.* **15**, 295–304 (2004).
3. Pierce, S. *et al.* A global method for calculating plant CSR ecological strategies applied across biomes world‐wide. *Funct. Ecol.* **31**, 444–457 (2017).
4. Díaz, S. *et al.* The global spectrum of plant form and function. *Nature* **529**, 167–171 (2016).
5. Stebbins, G. L. Aridity as a Stimulus to Plant Evolution. *Am. Nat.* **86**, 33–44 (1952).
6. Bohnert, H. J., Nelson, D. E. & Jensen, R. G. Adaptations to Environmental Stresses. *Plant Cell* **7**, 1099–1111 (1995).
7. Dai, A. Increasing drought under global warming in observations and models. *Nat. Clim. Chang.* **3**, 52–58 (2012).
8. Panchen, Z. A., Primack, R. B., Anisko, T. & Lyons, R. E. Herbarium specimens, photographs, and field observations show Philadelphia area plants are responding to climate change. *Am. J. Bot.* **99**,

751–756 (2012).

9. Primack, D., Imbres, C., Primack, R. B., Miller-Rushing, A. J. & Del Tredici, P. Herbarium specimens demonstrate earlier flowering times in response to warming in Boston. *Am. J. Bot.* **91**, 1260–1264 (2004).
10. Cleland, E. E., Chuine, I., Menzel, A., Mooney, H. A. & Schwartz, M. D. Shifting plant phenology in response to global change. *Trends Ecol. Evol.* **22**, 357–365 (2007).
11. Clausen, J., Keck, D. D. & Hiesey, W. M. Experimental studies on the nature of species. III. Environmental responses of climatic races of Achillea. *Experimental studies on the nature of species. III. Environresponses of climatic races of Achillea.* (1948).
12. Clausen, J. & Hiesey, W. M. Experimental studies on the nature of species. IV. Genetic structure of ecological races. *Experimental studies on the nature of species. IV. Genetic structure of ecological races.* (1958).
13. Lovell, J. T. *et al.* Pleiotropy of FRIGIDA enhances the potential for multivariate adaptation. *Proc. Biol. Sci.* **280**, 20131043 (2013).
14. Hereford, J. A quantitative survey of local adaptation and fitness trade-offs. *Am. Nat.* **173**, 579–588 (2009).
15. Sartori, K. *et al.* Leaf economics and slow-fast adaptation across the geographic range of Arabidopsis thaliana. *Sci. Rep.* **9**, 10758 (2019).
16. Willi, Y. & Van Buskirk, J. A review on trade-offs at the warm and cold ends of geographical distributions. *Philos. Trans. R. Soc. Lond. B Biol. Sci.* **377**, 20210022 (2022).
17. Merilä, J. Evolution. Genetic constraints on adaptation? *Science* vol. 325 1212–1213 (2009).
18. Etterson, J. R. & Shaw, R. G. Constraint to adaptive evolution in response to global warming. *Science* **294**, 151–154 (2001).
19. Ludlow, M. M. Strategies of response to water stress. (1989).
20. Dittberner, H. *et al.* Natural variation in stomata size contributes to the local adaptation of water-use

efficiency in Arabidopsis thaliana. *Mol. Ecol.* 4052–4065 (2018) doi:10.1111/mec.14838.

21. Franks, S. J., Sim, S. & Weis, A. E. Rapid evolution of flowering time by an annual plant in response to a climate fluctuation. *Proc. Natl. Acad. Sci. U. S. A.* **104**, 1278–1282 (2007).
22. Berger, J. D. & Ludwig, C. Contrasting adaptive strategies to terminal drought-stress gradients in Mediterranean legumes: phenology, productivity, and water relations in wild and domesticated Lupinus luteus L. *J. Exp. Bot.* **65**, 6219–6229 (2014).
23. Kooyers, N. J., Greenlee, A. B., Colicchio, J. M., Oh, M. & Blackman, B. K. Replicate altitudinal clines reveal that evolutionary flexibility underlies adaptation to drought stress in annual Mimulus guttatus. *New Phytologist* vol. 206 152–165 Preprint at https://doi.org/10.1111/nph.13153 (2015).
24. Paccard, A., Van Buskirk, J. & Willi, Y. Quantitative Genetic Architecture at Latitudinal Range Boundaries: Reduced Variation but Higher Trait Independence. *Am. Nat.* **187**, 667–677 (2016).
25. McKay, J. K., Richards, J. H. & Mitchell-Olds, T. Genetics of drought adaptation in Arabidopsis thaliana: I. Pleiotropy contributes to genetic correlations among ecological traits. *Mol. Ecol.* **12**, 1137–1151 (2003).
26. Juenger, T. E. *et al.* Identification and characterization of QTL underlying whole-plant physiology in Arabidopsis thaliana: delta13C, stomatal conductance and transpiration efficiency. *Plant Cell Environ.* **28**, 697–708 (2005).
27. Lasky, J. R. *et al.* Characterizing genomic variation of Arabidopsis thaliana: the roles of geography and climate. *Mol. Ecol.* **21**, 5512–5529 (2012).
28. Badiger, B. G. *et al.* Natural variation identifies new effectors of water use efficiency in Arabidopsis. *bioRxiv* 2022.03.28.486113 (2022) doi:10.1101/2022.03.28.486113.
29. Dammhahn, M., Dingemanse, N. J., Niemelä, P. T. & Réale, D. Pace-of-life syndromes: a framework for the adaptive integration of behaviour, physiology and life history. *Behav. Ecol. Sociobiol.* **72**, 62 (2018).
30. Farquhar, G. D., Hubick, K. T., Condon, A. G. & Richards, R. A. Carbon Isotope Fractionation and

Plant Water-Use Efficiency. in *Stable Isotopes in Ecological Research* 21–40 (Springer New York, 1989). doi:10.1007/978-1-4612-3498-2_2.

31. Wright, G. C., Hubick, K. T. & Farquhar, G. D. Discrimination in Carbon Isotopes of Leaves Correlates With Water-Use Efficiency of Field-Grown Peanut Cultivars. *Funct. Plant Biol.* **15**, 815–825 (1988).
32. Araus, J. L., Slafer, G. A., Reynolds, M. P. & Royo, C. Plant breeding and drought in C3 cereals: what should we breed for? *Ann. Bot.* **89 Spec No**, 925–940 (2002).
33. Seibt, U., Rajabi, A., Griffiths, H. & Berry, J. A. Carbon isotopes and water use efficiency: sense and sensitivity. *Oecologia* **155**, 441–454 (2008).
34. Ma, W. T., Yu, Y. Z., Wang, X. & Gong, X. Y. Estimation of intrinsic water-use efficiency from δ13C signature of C3 leaves: Assumptions and uncertainty. *Front. Plant Sci.* **13**, 1037972 (2022).
35. Kenney, A. M., McKay, J. K., Richards, J. H. & Juenger, T. E. Direct and indirect selection on flowering time, water-use efficiency (WUE, δ (13)C), and WUE plasticity to drought in Arabidopsis thaliana. *Ecol. Evol.* **4**, 4505–4521 (2014).
36. Le Corre, V., Roux, F. & Reboud, X. DNA polymorphism at the FRIGIDA gene in Arabidopsis thaliana: extensive nonsynonymous variation is consistent with local selection for flowering time. *Mol. Biol. Evol.* **19**, 1261–1271 (2002).
37. Fournier-Level, A. *et al.* Paths to selection on life history loci in different natural environments across the native range of Arabidopsis thaliana. *Mol. Ecol.* **22**, 3552–3566 (2013).
38. Kenney, A. M., McKay, J. K., Richards, J. H. & Juenger, T. E. Direct and indirect selection on flowering time, water-use efficiency (WUE, δ13C), and WUE plasticity to drought in Arabidopsis thaliana. *Ecol. Evol.* **4**, 4505–4521 (2014).
39. Monroe, J. G. *et al.* Drought adaptation in Arabidopsis thaliana by extensive genetic loss-of-function. *Elife* **7**, (2018).
40. Hall, M. C. & Willis, J. H. Divergent selection on flowering time contributes to local adaptation in

Mimulus guttatus populations. *Evolution* **60**, 2466–2477 (2006).

41. Franke, D. M. *et al.* A Steep Cline in Flowering Time for Brassica rapa in Southern California: Population‐Level Variation in the Field and the Greenhouse. *Int. J. Plant Sci.* **167**, 83–92 (2006).
42. Exposito-Alonso, M., Brennan, A. C., Alonso-Blanco, C. & Picó, F. X. Spatio-temporal variation in fitness responses to contrasting environments in Arabidopsis thaliana. *Evolution* (2018) doi:10.1111/evo.13508.
43. Exposito-Alonso, M. *et al.* Genomic basis and evolutionary potential for extreme drought adaptation in Arabidopsis thaliana. *Nat Ecol Evol* **2**, 352–358 (2018).
44. 1001 Genomes Consortium. 1,135 Genomes Reveal the Global Pattern of Polymorphism in Arabidopsis thaliana. *Cell* **166**, 481–491 (2016).
45. Seren, Ü. *et al.* AraPheno: a public database for Arabidopsis thaliana phenotypes. *Nucleic Acids Res.* **45**, D1054–D1059 (2017).
46. Philip Grime, J. & Pierce, S. *The Evolutionary Strategies that Shape Ecosystems*. (Wiley, 2012). doi:10.1002/9781118223246.
47. Delgado, D., Alonso-Blanco, C., Fenoll, C. & Mena, M. Natural variation in stomatal abundance of Arabidopsis thaliana includes cryptic diversity for different developmental processes. *Ann. Bot.* **107**, 1247–1258 (2011).
48. Martínez-Berdeja, A. *et al.* Functional variants of DOG1 control seed chilling responses and variation in seasonal life-history strategies in Arabidopsis thaliana. *Proc. Natl. Acad. Sci. U. S. A.* **117**, 2526–2534 (2020).
49. Atwell, S. *et al.* Genome-wide association study of 107 phenotypes in Arabidopsis thaliana inbred lines. *Nature* **465**, 627–631 (2010).
50. Wright, I. J. *et al.* The worldwide leaf economics spectrum. *Nature* **428**, 821–827 (2004).
51. Vasseur, F. *et al.* Adaptive diversification of growth allometry in the plant Arabidopsis thaliana. *Proc. Natl. Acad. Sci. U. S. A.* **115**, 3416–3421 (2018).

52. Debieu, M. *et al.* Co-variation between seed dormancy, growth rate and flowering time changes with latitude in Arabidopsis thaliana. *PLoS One* **8**, e61075 (2013).

53. Fick, S. E. & Hijmans, R. J. WorldClim 2: new 1-km spatial resolution climate surfaces for global land areas: NEW CLIMATE SURFACES FOR GLOBAL LAND AREAS. *Int. J. Climatol.* **37**, 4302–4315 (2017).

54. Fulgione, A. *et al.* Parallel reduction in flowering time from de novo mutations enable evolutionary rescue in colonizing lineages. *Nat. Commun.* **13**, 1461 (2022).

55. Simpson, G. G. & Dean, C. Arabidopsis, the Rosetta stone of flowering time? *Science* **296**, 285–289 (2002).

56. Méndez-Vigo, B., Picó, F. X., Ramiro, M., Martínez-Zapater, J. M. & Alonso-Blanco, C. Altitudinal and climatic adaptation is mediated by flowering traits and FRI, FLC, and PHYC genes in Arabidopsis. *Plant Physiol.* **157**, 1942–1955 (2011).

57. Elfarargi, A. F. *et al.* Genomic Basis of Adaptation to a Novel Precipitation Regime. *Mol. Biol. Evol.* **40**, (2023).

58. McKay, J. K., Richards, J. H. & Mitchell-Olds, T. Genetics of drought adaptation in Arabidopsis thaliana: I. Pleiotropy contributes to genetic correlations among ecological traits. *Mol. Ecol.* **12**, 1137–1151 (2003).

59. Brachi, B., Aimé, C., Glorieux, C., Cuguen, J. & Roux, F. Adaptive value of phenological traits in stressful environments: predictions based on seed production and laboratory natural selection. *PLoS One* **7**, e32069 (2012).

60. Mojica, J. P. *et al.* Genetics of water use physiology in locally adapted Arabidopsis thaliana. *Plant Sci.* **251**, 12–22 (2016).

61. Ågren, J., Oakley, C. G., Lundemo, S. & Schemske, D. W. Adaptive divergence in flowering time among natural populations of Arabidopsis thaliana: Estimates of selection and QTL mapping. *Evolution* (2016) doi:10.1111/evo.13126.

62. Manzano-Piedras, E., Marcer, A., Alonso-Blanco, C. & Picó, F. X. Deciphering the adjustment between environment and life history in annuals: lessons from a geographically-explicit approach in Arabidopsis thaliana. *PLoS One* **9**, e87836–e87836 (2014).

63. Fournier-Level, A. *et al.* A map of local adaptation in Arabidopsis thaliana. *Science* **334**, 86–89 (2011).

64. Exposito-Alonso, M. *et al.* Natural selection on the Arabidopsis thaliana genome in present and future climates. *Nature* **573**, 126–129 (2019).

65. Lande, R. & Arnold, S. J. The Measurement of Selection on Correlated Characters. *Evolution* **37**, 1210–1226 (1983).

66. Stearns, S. C. Trade-Offs in Life-History Evolution. *Funct. Ecol.* **3**, 259–268 (1989).

67. Kalladan, R. *et al.* Natural variation identifies genes affecting drought-induced abscisic acid accumulation in Arabidopsis thaliana. *Proc. Natl. Acad. Sci. U. S. A.* **114**, 11536–11541 (2017).

68. Vidigal, D. S. *et al.* Altitudinal and climatic associations of seed dormancy and flowering traits evidence adaptation of annual life cycle timing in Arabidopsis thaliana. *Plant Cell Environ.* **39**, 1737–1748 (2016).

69. Slovak, R. *et al.* A Scalable Open-Source Pipeline for Large-Scale Root Phenotyping of Arabidopsis. *Plant Cell* **26**, 2390–2403 (2014).

70. Lush, J. L. & Others. Animal breeding plans. *Animal breeding plans.* (1943).

71. Zhou, X. & Stephens, M. Genome-wide efficient mixed-model analysis for association studies. *Nat. Genet.* **44**, 821–824 (2012).

72. Zhou, X. & Stephens, M. Efficient multivariate linear mixed model algorithms for genome-wide association studies. *Nat. Methods* **11**, 407–409 (2014).

73. Kawakatsu, T. *et al.* Epigenomic Diversity in a Global Collection of Arabidopsis thaliana Accessions. *Cell* **166**, 492–505 (2016).

74. Ludlow, M. M. Strategies of response to water stress. in *Structural and functional responses to*

environmental stress (eds. Kreeb, K. H., Richter, H. & Minckley, T. M.) 269–281 (The Hague, the Netherlands: SPB Academic., 1989).

75. Stekhoven, D. J. & Bühlmann, P. MissForest--non-parametric missing value imputation for mixed-type data. *Bioinformatics* **28**, 112–118 (2012).

76. McCaw, Z. R., Lane, J. M., Saxena, R., Redline, S. & Lin, X. Operating characteristics of the rank-based inverse normal transformation for quantitative trait analysis in genome-wide association studies. *Biometrics* (2019) doi:10.1111/biom.13214.